# Fault Location in Meshed and Active Power Distribution Networks

Cesar Galvez, Ali Abur
Department of Electrical Engineering
Northeastern University
Boston, MA, USA
{galveznunez.c, abur}@ece.neu.edu

2021 IEEE Madrid PowerTech | 978-1-6654-3597-0/21/$31.00 ©2021 IEEE | DOI: 10.1109/PowerTech46648.2021.9494755

***Abstract*—This paper presents an effective fault location method for active distribution networks with radial and/or meshed typologies. Historically, most distribution networks have been radially configured and operated due to their passive characteristics containing no active power sources. However, recent increase in the number of Distributed Energy Resources (DERs) forced these networks to be configured and operated more like transmission systems containing meshed sections. This change presents several challenges one of which is detection and location of faults. This paper presents a practical and effective approach to address this challenge. It requires a limited number of digital fault recorders (DFR) to be placed and uses the Discrete Wavelet Transform (DWT) to compute the first arrival times of fault-generated traveling waves. Details of the proposed procedure are given in the paper. IEEE 123-Node Test Feeder is used to validate the method under different fault conditions using the EMTP RV program and Matlab as the simulation tools.**

***Keywords*—Fault location, Power System Faults, Electromagnetic Transients, Wavelet Transform, Traveling Waves.**

## I. Introduction

Massive penetration of Inverter-Based Power Sources (IBPS) or Distributed Energy Resources (DER) in distribution systems are inevitably changing the way these systems are operated and configured. Traditional radial configurations are replaced by meshed networks in order to exploit the reliability benefits of redundant paths to existing sources. Despite these advantages, they also pose challenges in terms of protection and fault location in such systems. Hence, innovative alternatives to conventional methods designed primarily for radial systems are needed.

Fault location methods can be classified into three categories: methods based on impedance measurements ( [1]- [2]), on traveling waves (TW) ( [3]- [4]) and artificial intelligence (AI) algorithms [5]. The methods based on AI are mostly used in the classification and identification of fault section [5]. The methods based on impedance measurement are broadly used in transmission lines but have some limitations caused by unknown fault resistances [6], asymmetry of lines, and in the presence of IBPS. On the other hand, the methods based on traveling waves remain robust against these factors. Besides, with the rapidly improving technology on the integrated optical sensors of voltage and current measurements, the TW method has become more attractive and practical to implement [7], [8]. The techniques in ( [9]- [10]) use the TW method to locate faults in meshed transmission networks via wide-area synchronized voltage measurements. The method presented in [11] and [12] can identify faults in radial networks, which are based on the computational difference of arrival times measured by DFRs. While quite effective, the applicability of these methods remain limited to detecting faults in strictly radial networks.

In this paper, the above limitation of these methods will be removed and an alternative approach that can detect and locate faults in radial as well as meshed networks will be presented. The proposed technique requires a DFR to be installed at each radial line terminal. These DFRs must be synchronized to capture the first arrival times of faulted voltage signals using Discrete Wavelet Transform (DWT). Arrival time differences are computed to obtain the closest bus to the faulted point using the minimum $\ell_2$-norm method. The incident edges and buses to the closest bus to the fault are then selected to determine the precise fault location using equations developed in sec. II-A3. The proposed method does not need the faulted section identification to determine the fault distance. Instead, it chooses a reference DFR and computes each selected edge's fault distance measured from the reference DFR, then by taking the maximum value from these estimated distances, determines the correct fault distance.

## II. Problem Formulation

The meshed distribution network shown in Fig. 1 will be used to describe the problem formulation. This system contains eight buses and two solar photovoltaic sources connected to 3-phase and single-phase laterals. The mixed network has four switches that connect via 3 phase lines to buses 6 and 8 as well as buses 5 and 8. When these four switches are open, the distribution network will be strictly radial, whereas it will becomes a meshed network with the switches closed. It is also assumed that there are four mixed-phase lateral lines of 3-phase, 2-phase and single-phase aerial line sections, and a 3-phase underground cable connected to the meshed network formed by the 3-phase overhead line in orange color. Four DFRs are placed at the terminal buses of the four laterals to capture the transient voltage signals. Even though the proposed

This work made use of Engineering Research Center Shared Facilities supported by the Engineering Research Center Program of the National Science Foundation and the Department of Energy under NSF Award Number EEC-1041877 and the CURENT Industry Partnership Program.

978-1-6654-3597-0/21/$31.00 ©2021 IEEE

method is illustrated using this radial-meshed distribution network, it can be readily applicable to transmission networks as well.

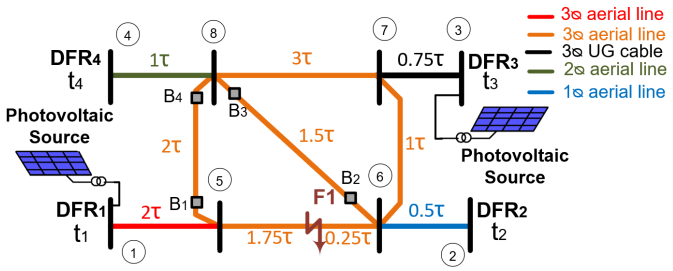


Fig. 1: Example Mixed Distribution Network

### A. *Fault Location Technique*

The fault location approach is implemented in two-steps. In the first step, the distribution network is represented as a weighted undirected graph, where edges represent the distribution lines and nodes represent the buses. Assuming that the lengths "$l$" and traveling wave speeds "$v$" of the distribution lines are known, the travel times $\tau$ for each line section can computed as $\tau = l/v = l\sqrt{L.C}$, where $L$ and $C$ are the per-unit length inductance and capacitance of the line for the considered mode. The computed travel times $\tau$ will be the weights in the modeled graph. The weighted graph is then used to estimate the closest bus to the faulted point, which will be referred as the faulted bus in the sequel. The second step involves the estimation of the accurate fault location. It involves selecting the incident edges and buses to the faulted bus, followed by the use of the shortest path rule to estimate the shortest travel time routes from incident buses to the nearest DFRs. These routes and incident edges establish fault location paths used in DFR pairs to calculate the precise fault distance.

#### 1) *Location of Bus closest to Faulted Point*

The first procedure assumes that the possible fault location occurs in any of the distribution network buses. Assume that the Digital Fault Recorders (DFRs) labeled as $DFR_i$, $i = 1, ..., 4$ are placed at line terminals and are all synchronized recorders. Let there be a fault F1 located in the line, close to bus 6, as depicted in fig.1. Likewise, assume that the $DFR2$ captured the first arrival time of fault-generated traveling waves, and the other DFRs register it later. Hence, the array $t_A$ containing the arrival times is formed and sorted in ascending order, as shown below.

$$t_A{}^T = \begin{matrix} DFR_2 & DFR_1 & DFR_3 & DFR4 \end{matrix} \\ \begin{bmatrix} t_2 & t_1 & t_3 & t_4 \end{bmatrix}$$

Using each line section's travel time build the theoretical travel time matrix "$\tau_t$," where the rows and columns correspond to buses with DFRs and all the system buses, respectively. The travel times between buses are determined using the shortest path approach established by the well-known Dijkstra's algorithm. Similar to the array ${t_A}^T$, the rows of the matrix are also ordered in ascending order following the same pattern of arrival times recorded by DFRs.

$$\tau_t = \begin{matrix} \\ 2 \\ 1 \\ 3 \\ 4 \end{matrix} \begin{matrix} \begin{matrix} 1 & 2 & .. & 6 & 7 & 8 \end{matrix} \\ \begin{bmatrix} \tau_{2.1} & 0 & ... & \tau_{2.6} & \tau_{2.7} & \tau_{2.8} \\ 0 & \tau_{1.2} & ... & \tau_{1.6} & \tau_{1.7} & \tau_{1.8} \\ \tau_{3.1} & \tau_{3.2} & ... & \tau_{3.6} & \tau_{3.7} & \tau_{3.8} \\ \tau_{4.1} & \tau_{4.2} & ... & \tau_{4.6} & \tau_{4.3} & \tau_{4.8} \end{bmatrix} \end{matrix}$$

As the DFR2 registers the first arrival time, it is selected as the reference to form the measured shortest travel time array ${\tau_m}^T$, which is determined by taking the time differences between the arrival time of DFR2 and all the other DFRs, as shown (1).

$${\tau_m}^T = \begin{bmatrix} \tau_{1.2}^{(m)} & \tau_{3.2}^{(m)} & \tau_{4.2}^{(m)} \end{bmatrix} \tag{1}$$

where $\tau_{1.2}^{(m)}$, $\tau_{3.2}^{(m)}$, and $\tau_{4.2}^{(m)}$ are the measured travel times of the fault signal with respect to the first arrival time $t_2$. As an illustration, $\tau_{1.2}^{(m)}$ can be represented by $\tau_{1.2}^{(m)} = \tau_{1.f} - \tau_{2.f}$, where $\tau_{1.f}$, and $\tau_{2.f}$ are the travel time differences from buses 1 and 2 to the faulted point. A similar procedure is followed using the matrix $\tau_t$ and selecting bus 2 as the reference in row 1 to form the theoretical travel time difference matrix $\Delta\tau_t$, as depicted in (2).

$$\Delta\tau_t = \begin{bmatrix} -\Delta\tau_{2.1} & \Delta\tau_{1.2} & .. & \Delta\tau_{1.6-2.6} & \Delta\tau_{1.7-2.7} & \Delta\tau_{1.8-2.8} \\ \Delta\tau_{3.1-2.1} & \Delta\tau_{3.2} & .. & \Delta\tau_{3.6-2.6} & \Delta\tau_{1.7-2.7} & \Delta\tau_{3.8-2.8} \\ \Delta\tau_{4.1-2.1} & \Delta\tau_{4.2} & .. & \Delta\tau_{4.6-2.6} & \Delta\tau_{1.7-2.7} & \Delta\tau_{4.8-4.8} \end{bmatrix} \tag{2}$$

A new travel time difference matrix can then be formed by subtracting the vector ${\tau_m}^T$ from each column of $\Delta\tau_t$, as given by (3).

$$\Delta\tau_x = \Delta\tau_t - {\tau_m}^T \tag{3}$$

Now, the matrix $\Delta\tau_x$ can be used in identifying the closest bus to the fault because it will match the measured time differences registered by synchronized DFRs with the theoretical shortest traveling time differences computed between the fault and each recording point. Therefore, calculating the $\ell_2$-norm for each column in the matrix $\Delta\tau_x$ and selecting the minimum will yield the bus closest to the fault point.

$$\ell_x = Min(\|\Delta\tau_x\|_2;\ x \in \{1, 2, ...., N\}) \tag{4}$$

where $x$ represents the faulted bus and N is the number of buses in the distribution network. For the case of Fig. 1, $x = 6$ and $N = 8$. As aforementioned, this first method assumes that fault occurs at a system bus. However, it is well known that faults are more likely to happen along the lines rather than at buses. Hence, this assumption needs to be relaxed and a more general approach needs to be developed which is presented next.

#### 2) *Evaluating the Accurate Fault location*

The distribution network of Fig. 1 can be modeled as a weighted undirected graph, as shown in Fig. 2. Let us consider a fault at point F1, which will initiate traveling waves that travel along both directions of distribution line and will reach

the DFRs following the shortest path. Assume that F1 is $0.25\tau$ away from bus 6. Note that using the previous method of the minimum $\ell_2$-norm will yield bus 6 as the closest bus to the fault. However, the second minimum norm will yield bus 2 instead of bus 5 because the travel time $\tau_{2.6} = 0.5\tau$ is shorter than the travel time from the fault to bus 5 $\tau_{5.F} = 1.75\tau$. Hence, relying on the two minimum norms to identify the faulted section will lead to the wrong fault location. Instead, the proposed method first localizes the bus closest to the fault (faulted bus) and then selects the incident edges and buses to the faulted bus to estimate the precise fault location. For the F1 fault case, the green edges and circles marked in Fig. 2 are selected as incident edges and buses to the faulted bus 6. The proposed approach does not need to identify the faulted line section because it will evaluate all incident edges connected to the faulted bus, as shown in Fig.2.

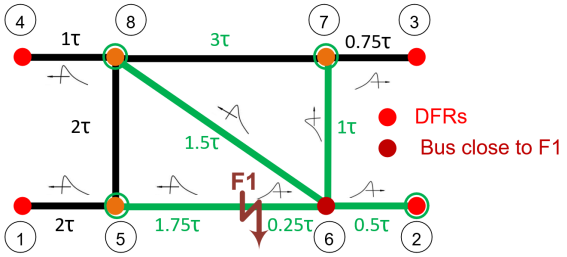


Fig. 2: Weighted Indirected Graph

As previously shown, the incident edges and buses to the faulted bus are already known. When the fault occurs, the fault-generated traveling waves travel along the incident edges and exit through the incident buses to reach the nearest DFRs following the shortest travel routes. Applying this logic it is possible to determine the distances, routes, and the DFRs having the first arrival times observed from each incident bus. For example, $DFR_2$ records the first arrival time from the incident bus 2, $DFR_1$ captures the first arrival time from the incident bus 5, and the same process is repeated for the rest of the DFRs. Note that the distribution network is a weighted undirected graph. Hence, disregarding the faulted bus virtually ensures that the fault always travels forward to reach the nearest DFR. The fault distance can then be estimated by assuming a reference DFR and forming pairs among the reference DFR and the other DFRs placed at line terminals.

### *3) Determining the Fault Occurrence Time $t_f$, Faulted Section $s$ and Fault Distance X*

Knowing the first arrival times and travel routes of fault to reach the DFRs, the weighted undirected graph can then be modeled as a radial distribution system as shown in fig. 3. As seen in fig 3, the radial distribution network includes only the lines in which the fault travels to reach the closest DFRs following the shortest route rule. This reduced system is used to derive the fault occurrence time $t_f$ for F1 fault occurring along the main feeder. It is assumed that the system places DFRs in each line terminal and the DFR1 is selected as

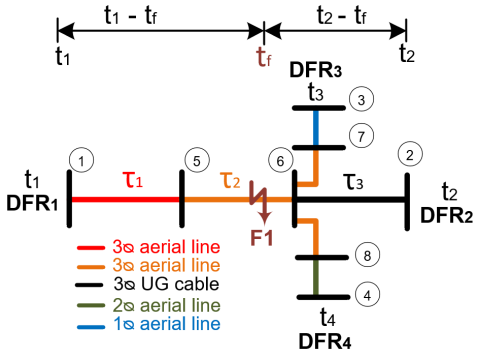


Fig. 3: Radial Distribution System

the reference DFR. This distribution system includes a main feeder composed of 3 phase overhead lines and a 3-phase underground cable. Additionally, it has two lateral lines of 2-phase and a single-phase connected to bus 6. The voltage traveling wave signals generated by F1 are captured by $DFR_1$ and $DFR_2$ to extract the arrival times $t_1$ and $t_2$ using Discrete Wavelet Transform (DWT). Note that the theoretical traveling times for each line section $\tau_i$, and the arrival times $t_1$ and $t_2$ can be used in (5) to estimate the unknown fault occurrence time ($t_f$).

$$t_f = \frac{1}{2}(t_1 + t_2 - \sum_{i=1}^{N} \tau_i) \tag{5}$$

where $t_1$ and $t_2$ are the arrival times at buses 1 and 2. $\tau_i$ are the travel times computed theoretically for each line section from bus 1 to bus 2. $N$ is the number of the line sections; for the case of Fig.3 $N = 3$. The fault occurrence time $t_f$ is utilized in the identification of the faulted section $s$, which is necessary to determine the fault distance selecting $DFR_1$ as the reference. The unknown faulted section can be found when the next condition given by (6) is satisfied.

$$t_1 - t_f \leq \sum_{i=1}^{s} \tau_i \tag{6}$$

The first $s$ that satisfies the condition (6) will be the faulted section, which is used in the estimation of the fault distance $X$ given by (7). $X$ is derived by using the $DFR_1$ reference, but it can also be estimated by selecting another existing DFR as the reference in the distribution network. Note that $X$ will be estimated by $X = V_1(t_1 - t_f)$ for $s = 1$. Otherwise, for $s \geq 2$, $X$ will be determined by the equation (7).

$$X = V_s(t_1 - t_f - \sum_{i=1}^{s-1} \tau_i) + \sum_{i=1}^{s-1} V_i \tau_i \tag{7}$$

where $s$ is the faulted section, $V_s$ is the faulted section aerial modal speed (mode 1) and $\tau_i$ and $V_i$ are the travel times and aerial modal speed for each feeder section $i$.

### *4) Locating Faults at any Point in the Network*

The above analysis assumes that fault is located in the main feeder, but it can also be found in the lateral branches. Hence, the three previous equations should be generalized to work for

faults located at any arbitrary point in the distribution network. The number of possible DFR pairs $n$ to be formed in the network is given by $n = k-1$, where $k$ is the number of DFRs, e.g. $n = 3$ in fig. 3. Clearly, $n$ should be repeated $n$ times in order to estimate the fault occurrence time $t_{f_{(R,j)}}$ and it can be calculated using (8), where $R = 1$ and $j = 2, ..., k = 4$.

$$t_{f_{(R,j)}} = \frac{1}{2}(t_R + t_j - \sum_{i=1}^{N_{(R,j)}} \tau_i) \tag{8}$$

As the fault occurrence times $t_{f_{(R,j)}}$ are computed $n$ times, these times should be stored in the array $T_{DFR_1}$. Thus, extracting the minimum value from $T_{DFR_1}$ will provide the fault occurrence time given by (9).

$$T_{DFR1} = DFR_1 \begin{bmatrix} DFR_1 & DFR_2 & DFR_3 & ... & DFR_k \\ - & t_{f1.2} & t_{f1.3} & ... & t_{f1.k} \end{bmatrix}$$

$$t_{f_{DFR_1}} = \min_u(T_{DFR1}(u)) \tag{9}$$

The faulted section $s$ should also be estimated by each DFR pair and it can be computed by (10). Similar to the fault occurrence time array $T_{DFR1}$, the faulted sections are stored in the array $S_{DFR1}$ shown below.

$$t_R - t_{f_{(R,j)}} \leq \sum_{i=1}^{s_{(R,j)}} \tau_i \tag{10}$$

$$S_{DFR1} = DFR_1 \begin{bmatrix} DFR_1 & DFR_2 & DFR_3 & ... & DFR_k \\ - & S_{1.2} & S_{1.3} & ... & S_{1.k} \end{bmatrix}$$

Using the fault occurrence times and faulted sections stored in $T_{DFR_1}$ and $S_{DFR_1}$ arrays, the fault distance $X_{(R,j)}$ can easily be computed by (11) when $s_{(R,j)} = 1$. On the other hand, if $s_{(R,j)} >= 2$, $X_{(R,j)}$ must be determined by (12), where $R = 1$ and $j$ refers to the other DFRs $j = 2, 3, ..k$. Similar to the two previous arrays, the fault distances $X_{(R,j)}$ computed $n$ times are stored in the array $X_{DFR1}$, then by taking the maximum value in $X_{DFR1}$ will yield the accurate fault distance and route, as shown in (13).

$$X_{(R,j)} = V_{s(R,j)}(t_R - t_{f_{(R,j)}}) \tag{11}$$

$$X_{(R,j)} = V_{s(R,j)}(t_R - t_{f_{(R,j)}} - \sum_{i=1}^{s_{(R,j)}-1} \tau_i) + \sum_{i=1}^{s_{(R,j)}-1} V_i \tau_i \tag{12}$$

$$X_{DFR_1} = DFR_1 \begin{bmatrix} DFR_1 & DFR_2 & DFR_3 & ... & DFR_k \\ - & X_{1.2} & X_{1.3} & ... & X_{1.k} \end{bmatrix}$$

$$X = \max_u(X_{DFR1}(u)) \tag{13}$$

## III. Practical Implementation

### A. Initial Considerations

All the distribution line sections are modeled using Frequency Dependent(FD) distributed lines [13] and are assumed to be non-transposed. The 3-phase measured voltage waveforms are transformed into decoupled modal signals to be evaluated independently using the Clarke transformation matrix [14]. The Discrete Wavelet Transform (DWT) decomposes the voltage modal components into five levels through the mother wavelet Daubechies3 (DB3) [15], [16]. The wavelet transform coefficient (WTC) at level 1 (D1) are processed to extract the first arrival times due to its ample high-frequency content. Besides, WTCs are squared to obtain $(WTC)^2$ in order to reduce the effect of noise in the signal.

### B. Simulation Model

The IEEE 123 Node Test Feeder [17] shown in Fig.4 is used to test the proposed fault location method. Closing the breakers in green color converts the distribution system into a meshed network. Four single-phase PV units are connected to the system via inverters, constituting Inverter Based Power Sources (IBPSs). Each IBPS provides 20 KVA to the grid in power factor control mode, set at 0.95PF. The Average Value Model (AVM) type converter utilized in this simulation can be found in [18]. As this meshed network contains many lateral lines connected to the main feeder, installing DFRs only in terminal buses of these laterals will enable the identification of any fault in the system as also done in [19]. Hence, sixteen DFRs are placed at line terminals, six of which are 3-phase, and the rest are single-phase. Note that this method does not need all the placed DFRs in the system. Instead, it relies on a small number of DFRs that are closest to the fault with the shortest travel routes. Thus, any changes in network topology will not have an impact on the precision unless they occur along any of these travel routes. A sampling frequency of 11 MHz is used for the time-domain simulations. No DFRs are placed for very short length lines. However, if a fault occurs in these short lateral lines, the proposed algorithm will observe the fault as occurring at the junction where the faulted lateral connects to the main feeder. Two cases will be discussed in detail to illustrate the precision of proposed method.

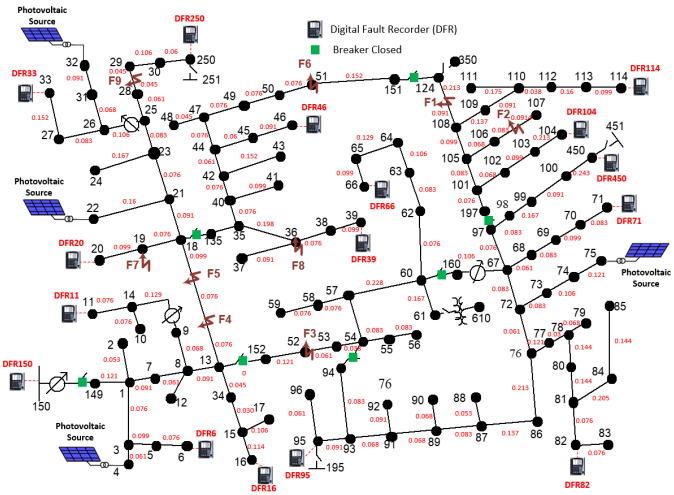


Fig. 4: IEEE 123 Test Node Feeder.

### C. Simulation Results

#### 1) *Case 1: DLG Fault at 0.091 km Away From Bus 108*

Consider a double-line-to-ground (DLG) fault F1 as shown in Fig. 4 occurring at 0.091 km away from bus 108 on a 0.3048 km long line connecting buses 105 and 108, with

TABLE I: **Arrival Times(ms) for faults F1 and F2**

| DFR | ToA$_{F1}$ | ToA$_{F2}$ | DFR | ToA$_{F1}$ | ToA$_{F2}$ |
|---|---|---|---|---|---|
| DFR114 | 30.692 | 33.4725 | DFR39 | 30.6941 | 33.4753 |
| DFR104 | 30.6921 | 33.472 | DFR150 | 30.6948 | 33.4747 |
| DFR71 | 30.6926 | 33.4723 | DFR11 | 30.6948 | 33.4748 |
| DFR46 | 30.6927 | 33.4738 | DFR250 | 30.6952 | 33.4763 |
| DFR450 | 30.6931 | 33.4729 | DFR6 | 30.6953 | 33.4752 |
| DFR95 | 30.6934 | 33.4733 | DFR33 | 30.6954 | 33.4764 |
| DFR82 | 30.6936 | 33.4734 | DFR66 | 30.6961 | 33.476 |
| DFR20 | 30.6939 | 33.475 | DFR16 | 30.6943 | 33.4741 |

a fault resistance 10Ω and fault inception angle of 30°. The inception time of fault is set at $30.69ms$. The 3-phase fault-generated voltage signals are decoupled into their modal components using Clarke Transformation. The modal voltage signals (mode 1) are then processed via Wavelet Transform Discrete ($DWT$) to obtain the Squared Wavelet Transform Coefficients ($WTC^2$), which are used to compute the first arrival times as shown in table I. The minimum $\ell_2$-norm method uses the arrival times captured by DFRs to determine the closest bus to the faulted point. The bus 108 has the minimum $\ell_2$-norm, demonstrating that the fault F1 is closest to bus 108, as depicted in Fig. 5. The next step is to identify the incident edges and buses to bus 108.

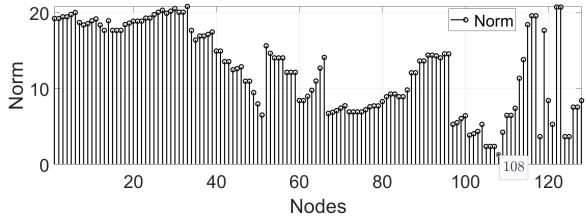


Fig. 5: $\ell_2$-Norm Estimation For Fault F1

As shown in Fig. 6, the incident edges are the lines 108-124, 108-109 and 108-105. Likewise, the incident buses to the faulted bus 108 are 105, 109 and 124. Using the shortest travel time route method and artificially ignoring the faulted bus, the DFRs closest to the three incident buses are found as DFR104, DFR114 and DFR46 respectively. Any of three DFRs can be selected as the reference DFR. For example, let us choose the DFR114 to be the reference DFR in this evaluation. The reference DFR and the other two DFRs form pairs. Thefore, using (8) for the reference DFR and its pairs, the fault occurrence time array $T_{DFR}$ can be calculated as shown below.

$$T_{DFR} = \begin{matrix} \\ DFR_{114} \end{matrix} \begin{matrix} \begin{matrix} DFR_{114} & DFR_{104} & DFR_{46} \end{matrix} \\ \begin{bmatrix} - & 30.6902 & 30.69 \end{bmatrix} \end{matrix}$$

Extracting the minimum value from the $T_{DFR}$ array will yield the accurate fault occurrence time $t_f$ of $30.69ms$. Besides, the faulted section array $S_{DFR}$ for the reference DFR and its pairs are computed by using (10), which yields $s = 1$ because the routes among the selected DFRs are formed only by overhead distribution lines.

$$S_{DFR} = \begin{matrix} \\ DFR_{114} \end{matrix} \begin{matrix} \begin{matrix} DFR_{114} & DFR_{104} & DFR_{46} \end{matrix} \\ \begin{bmatrix} - & 1 & 1 \end{bmatrix} \end{matrix}$$

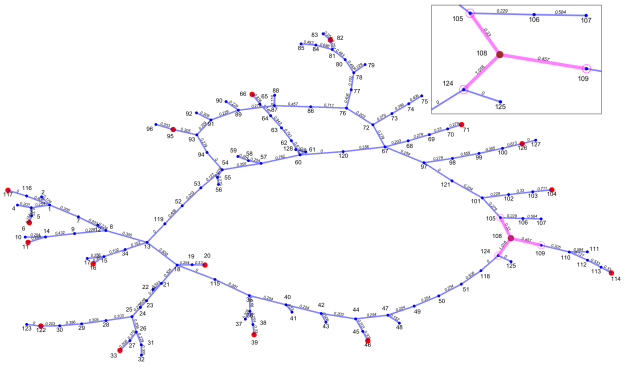

Fig. 6: Weighted Undirected Graph For Fault F1

Both $T_{DFR}$ and $S_{DFR}$ arrays are used to determine the fault distance arrays $X_{DFR}$ computed by (11). In the case the fault is located in a line-cable hybrid distribution line, the faulted section will be $s = 2$, and the fault distance will be determined by (12).

$$X_{DFR} = \begin{matrix} \\ DFR_{114} \end{matrix} \begin{matrix} \begin{matrix} DFR_{114} & DFR_{104} & DFR_{46} \end{matrix} \\ \begin{bmatrix} - & 0.529 & 0.6159 \end{bmatrix} \end{matrix}$$

Extracting the maximum value from the fault distance array $X_{DFR}$ will correspond to the precise fault distance $X$, which is 0.6159 km and comparing it with the actual distance of 0.616km, the estimated error is found as 0.0162%.

*2) **Case 2**: SLG Fault at 0.0914 km Away From Bus 107*

A single-line to ground (SLG) fault F2 shown in Fig. 4 occurs at 0.0914 km away from bus 104 on a 0.175 km long single-phase line connecting buses 106 and 107. The fault resistance and angle are set to 20Ω and 90°. The fault inception time is set at $33.47ms$. The first arrival times generated by the transient voltage signals are captured by DFRs as shown in table I. The minimum $\ell_2$-norm method uses these arrival times to identify the closest bus to the faulted point. It yields the buses 105, 106 and 107 with the same minimum norms, as depicted in Fig. 7. This happens because there is no DFR installed at the single-phase faulted lateral line terminal. However, the proposed method will still identify the faulted lateral by identifying the buses with the minimum norms.

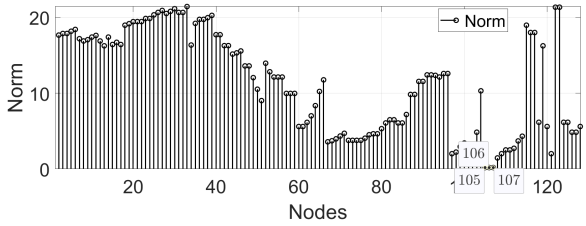


Fig. 7: $\ell_2$-Norm Estimation For Fault F2

As the minimum $\ell_2$-norms are the same for buses 105, 106, and 107, it can be concluded that the short-circuit is located in the lateral line connected to bus 105. To verify this result, we can calculate the fault distance using the closest DFRs to bus 105, which are the DFRs 104 and 114, as shown in

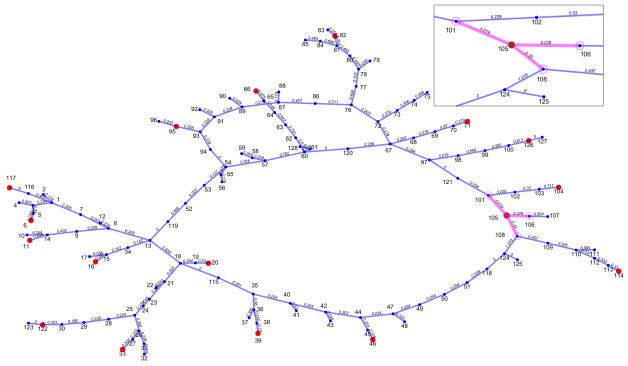

Fig. 8: Weighted Undirected Graph For Fault F2

Fig. 8. Considering the DFR104 as the reference DFR, the fault distance array $X_{DFR}$ for the DFR pair 104 and 114 can be estimated. The estimated distance of 0.4645km from the reference DFR104 verifies that the proposed method observes the fault as occurring at the junction connecting the faulted lateral.

$$X_{DFR} = \begin{matrix} \\ DFR_{104} \end{matrix} \begin{matrix} \begin{matrix} DFR_{104} & DFR_{144} \end{matrix} \\ \begin{bmatrix} - & 0.4645 \end{bmatrix} \end{matrix}$$

### D. *Proposed Method Performance Under Different Fault Conditions*

This section presents a summary considering different fault conditions shown in Fig. 4, such as fault type, fault resistance, fault inception angle, as well as including non-transposed cable and line sections and Inverter-Based Power Sources (IBPSs) to the distribution network. The simulation results corresponding to the distances shown in Fig.4 yield maximum and average errors of 0.083% and 0.0607%, as shown in table II. These results show that the network configuration and types of faults do not affect the proposed method's fault location performance.

TABLE II: **Errors of Fault Location.**

| Fault | Location | Rf | Fault Angle | Fault Type | Error(%) |
|---|---|---|---|---|---|
| F3 | Bus52 | 10Ω | 135° | ABC-g | 0.053% |
| F4 | 30.27% $L_{13-18}$ | 20Ω | 60° | BC | 0.083% |
| F5 | 60.55% $L_{13-18}$ | 40Ω | 10° | AB-g | 0.067% |
| F6 | Bus51 | 30Ω | 45° | ABC | 0.052% |
| F7 | Bus19 | 50Ω | 90° | A-g | 0.0586% |
| F8 | Bus36 | 60Ω | 90° | B-g | 0.036% |
| F9 | 50% $L_{28-29}$ | 50Ω | 135° | BC-g | 0.0753% |

## IV. Conclusion

This paper proposes a fault location method for meshed distribution networks that remains robust against unknown fault resistance, asymmetry of the distribution lines, and the presence of Inverter-Based Power Sources (IBPSs) connected to the distribution system. This approach can easily locate faults regardless of its location in the meshed network. It does not require the faulted section identification. Instead, the algorithm identifies the closest bus to the faulted point and selects its incident edges and buses to compute the accurate fault location. Future work will investigate the use of this application for meshed transmission networks using a reduced number of DFRs.

## References


[1] M. S. Sachdev and R. Agarwal, "A technique for estimating transmission line fault locations from digital impedance relay measurements," *IEEE Transactions on Power Delivery*, vol. 3, no. 1, pp. 121–129, Jan 1988.

[2] E. Styvaktakis, M. H. J. Bollen, and I. Y. H. Gu, "A fault location technique for two and three terminal lines using high frequency fault clearing transients," in *PowerTech Budapest 99. Abstract Records. (Cat. No.99EX376)*, Aug 1999, pp. 255–.

[3] F. H. Magnago and A. Abur, "Fault location using wavelets," *IEEE Transactions on Power Delivery*, vol. 13, no. 4, pp. 1475–1480, 1998.

[4] C. Y. Evrenosoglu and A. Abur, "Travelling wave based fault location for teed circuits," *IEEE Transactions on Power Delivery*, vol. 20, no. 2, pp. 1115–1121, 2005.

[5] A. Yadav and A. Swetapadma, "Enhancing the performance of transmission line directional relaying, fault classification and fault location schemes using fuzzy inference system," *IET Generation, Transmission Distribution*, vol. 9, no. 6, pp. 580–591, 2015.

[6] A. D. Filomena, R. H. Salim, M. Resener, and A. S. Bretas, "Ground distance relaying with fault-resistance compensation for unbalanced systems," *IEEE Transactions on Power Delivery*, vol. 23, no. 3, pp. 1319–1326, July 2008.

[7] J. Ding, X. Wang, Y. Zheng, and L. Li, "Distributed traveling-wave-based fault-location algorithm embedded in multiterminal transmission lines," *IEEE Transactions on Power Delivery*, vol. 33, no. 6, pp. 3045–3054, 2018.

[8] S. Xie, Y. Zhang, H. Yang, H. Yu, Z. Mu, C. Zhang, S. Cao, X. Chang, and R. Hua, "Application of integrated optical electric-field sensor on the measurements of transient voltages in ac high-voltage power grids," *Applied Sciences*, vol. 9, no. 9, p. 1951, 2019.

[9] M. Korkali, H. Lev-Ari, and A. Abur, "Traveling-wave-based fault-location technique for transmission grids via wide-area synchronized voltage measurements," *IEEE Transactions on Power Systems*, vol. 27, no. 2, pp. 1003–1011, 2012.

[10] M. Korkali and A. Abur, "Fault location in meshed power networks using synchronized measurements," in *North American Power Symposium 2010*, 2010, pp. 1–6.

[11] S. Robson, A. Haddad, and H. Griffiths, "Fault location on branched networks using a multiended approach," *IEEE Transactions on Power Delivery*, vol. 29, no. 4, pp. 1955–1963, Aug 2014.

[12] R. Chen, X. Yin, X. Yin, Y. Li, and J. Lin, "Computational fault time difference-based fault location method for branched power distribution networks," *IEEE Access*, vol. 7, pp. 181 972–181 982, 2019.

[13] J. R. Marti, "Accurate modelling of frequency-dependent transmission lines in electromagnetic transient simulations," *IEEE Transactions on Power Apparatus and Systems*, vol. PAS-101, no. 1, pp. 147–157, 1982.

[14] H. W. Dommel, *EMTP theory book*. Microtran Power System Analysis Corporation, 1996.

[15] S. Santoso, E. J. Powers, W. M. Grady, and P. Hofmann, "Power quality assessment via wavelet transform analysis," *IEEE transactions on Power Delivery*, vol. 11, no. 2, pp. 924–930, 1996.

[16] I. Daubechies, *Ten lectures on wavelets*. Siam, 1992, vol. 61.

[17] IEEE, "IEEE 34 Test Node Feeder," http://sites.ieee.org/pes-testfeeders/resources/, 2008, [Corrections; 17 Sept 2010].

[18] U. Karaagac, J. Mahseredjian, R. Gagnon, H. Gras, H. Saad, L. Cai, I. Kocar, A. Haddadi, E. Farantatos, S. Bu, K. W. Chan, and L. Wang, "A generic emt-type model for wind parks with permanent magnet synchronous generator full size converter wind turbines," *IEEE Power and Energy Technology Systems Journal*, vol. 6, no. 3, pp. 131–141, Sep. 2019.

[19] C. Galvez and A. Abur, "Fault location in active distribution networks containing distributed energy resources (ders)," *IEEE Transactions on Power Delivery*, pp. 1–1, 2020.